JST: Smart Systems and Devices
Volume 35, Issue 2, May 2025, 017-024

Application of Neural Network in Predicting Optimization of Axisymmetric Boattail Angle for Drag Reduction

Tran The Hung[1*], Dao Cong Truong[2], Le Dinh Anh[3], Nguyen Trang Minh[2], Dinh Cong Truong[4]
[1]*Faculty of Aerospace Engineering, Le Quy Don Technical University, Ha Noi, Vietnam*
[2]*AMST, Le Quy Don Technical University, Ha Noi, Vietnam*
[3] *University of Engineering and Technology, Vietnam National University, Hanoi, Ha Noi, Vietnam*
[4]*School of Mechanical Engineering, Hanoi University of Science and Technology, Ha Noi, Vietnam*
[*]*Corresponding author email: tranthehung_k24@lqdtu.edu.vn*

Abstract

The study tries to classify the axisymmetric boattail models with minimum drag using numerical simulation and neural networks. Numerical simulation was conducted for the boattail model in a range of angles from 0 to 22°and length from 0.5 to 1.5 diameter of the model. The Mach number was changed from 0.1 to 3.0. The results revealed that, the angle with minimum drag is around 14° at subsonic but it dramatically shifts to 7-9° at supersonic conditions. The maximum error of the neural network in predicting aerodynamic drag is less than 2%. At subsonic flow, the angle with minimum drag is around 14° and boattail length was 1.5 times the model diameter. At supersonic conditions, the angle and length are around 7° and 1.5 diameter of the model, respectively. Increasing boattail length results in reducing drag. This study provides a good reference for further design of flying objects and proposes control method for drag reduction.

Keywords: Axisymmetric blunt body, boattail, drag reduction, ANN, wake structure.

1. Introduction

Blunt-based model is a common object in aerospace engineering as well as for practical applications such as building or bridges. This kind of model features a large separation behind the base, which results in high aerodynamic drag. To reduce the drag, modification of the model is required. Among the techniques for drag reduction, boattail shows a high effectiveness. The boattail is understood as an additional conical geometry added to the base. By reducing the base area, the drag can be reduced. However, drag reduction highly depends on the boattail geometry, which includes both the angles, length, and velocity conditions [1-4].

In various studies by Tran *et al*. [1, 2], a numerical method was applied to calculate the drag behavior of the axisymmetric model acquired with 0.7-diameter conical boattail at both subsonic and supersonic conditions. In those studies, a traditional method was applied to solve the Navier-Stokes equation for drag. Although this method is sufficiently powerful for aerodynamic force and surface flow, it is quietly expensive with many steps for simulation. The other approach is used by experimental studies, which were conducted by Mariotti *et al*. [5] and Tran *et al*. [6] for axisymmetric boattail models. However, the approach is not suitable in Vietnam due to the lack of wind tunnel facilities. Consequently, other methods are required to develop for further studies.

In recent years, the significant advancement of Artificial Neural Networks (ANNs) has transformed various aspects of the aerospace industry. Particularly notable is their application in predicting aerodynamic coefficients of flying objects, a field that has attracted considerable attention. ANNs, with their ability to learn from extensive and complex datasets, have become essential tools for this task. By leveraging data that includes the geometric and physical attributes of flying objects, as well as insights from simulations and flight tests, ANNs proficiently learn and predict aerodynamic coefficient values with remarkable accuracy. The use of ANNs in aerodynamic coefficient prediction not only streamlines the aircraft design process, reducing both time and costs but also provides deep insights into the factors influencing flight performance. This enables designers and engineers to enhance aircraft designs, optimizing performance metrics such as fuel efficiency while maintaining high standards of safety and reliability during operation. Thirumalainambi *et al*. [7], for example, examined the influence of activation functions and input data quantity on the predictive capabilities of ANNs for aerodynamic coefficients. The study found that with sufficient data, ANNs could effectively predict

ISSN 2734-9373
https://doi.org/10.51316/jst.182.ssad.2025.35.2.3
Received: Oct 24, 2024; revised: Feb 24, 2025
accepted: Apr 15, 2025

complex aerodynamic coefficients such as drag, lift, and moment. Consequently, the sigmoid function in the hidden layer is the most suitable for a 3-layer ANN in the predictions of the aerodynamic parameters.

In this study, a numerical process was presented to generate data for predicting the aerodynamic drag of an axisymmetric model with different boattail configurations. The simulation was conducted using Reynolds-averaged Navier-Stokes equations and the flow around the model was validated and discussed. A neural network was then developed to predict aerodynamic drag based on the acquired data. The results indicate that the proposed ANN achieves high accuracy, with an uncertainty of less than 2%. Additionally, it was confirmed that the boattail angle significantly influences the drag trend, whereas the boattail length contributes to drag reduction. Notably, the boattail model with the least drag shifts sharply from 14° to 7° when the flow transitions from subsonic to transonic and supersonic conditions.

2. Numerical Method

2.1. Model Geometry

The geometry of the model is shown in Fig. 1. In the details, it has a diameter (D) of 57 mm and a total length of 5D. The nose of the model has an ogive shape with a length of 2D while the main body has a cylinder shape. The selection of the shape of the nose presents a large change of drag from subsonic to supersonic conditions. As a result, it is much easier to compare the outcome for a wide range of Mach numbers. The afterbody has a conical shape with changeable length and angles. The definition of boattail angle β can be seen from Fig. 1. The model is similar to the previous study by Platou *et al*. [8]. However, the boattail length can be changed in the current study.

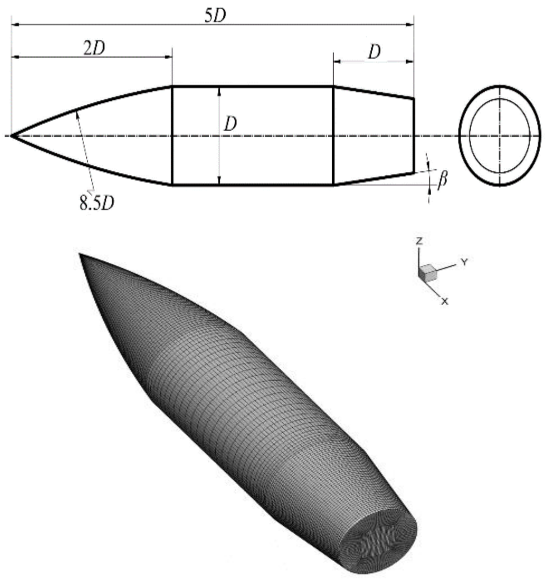

Fig. 1. Research model and mesh around the model

2.2. Numerical Scheme

In this study, the Reynolds-averaged Navier-Stokes (RANS) equations with the *k-ω* SST turbulence model are applied for numerical simulations. This model combines the *k-ω* model for near-wall flow and the *k-ε* model for far-wall flow. The *k-ω* SST turbulence model incorporates two additional turbulence equations, *k-ε,* and *k-ω*, to simulate turbulence characteristics, allowing for highly accurate results near the surface of the object and reducing computational time in numerical simulations. To derive the RANS equations, the averaging process is applied to the Navier-Stokes equations, including the continuity equation, the three momentum equations, and the energy equation. Specifically, the RANS model can be represented as follows [9]:

$$\frac{\partial \rho}{\partial t}+\frac{\partial}{\partial x_i}\left(\rho u_i\right)=0 \tag{1}$$

$$\begin{aligned}&\frac{\partial}{\partial t}\left(\rho u_i\right)+\frac{\partial}{\partial x_j}\left(\rho u_i u_j\right)=-\frac{\partial p}{\partial x_i}+\\&\mu\frac{\partial}{\partial x_j}\left(\frac{\partial u_i}{\partial x_j}+\frac{\partial u_j}{\partial x_i}\right)+\frac{\partial}{\partial x_j}\left(-\rho u_i^{'} u_j^{'}\right)\end{aligned} \tag{2}$$

where: i, j = 1, 2, 3; u_i is the average velocity component in each direction, p is pressure, ρ is the air density, and σ_{ij} is the stress tensor component; $-\rho u_i^{'} u_j^{'}$ is Reynolds Shear Stress. Equations for k and ω are:

$$\begin{aligned}&\frac{\partial(\rho k)}{\partial t}+\frac{\partial\left(\rho u_j k\right)}{\partial x_j}=P+\beta^*\rho\omega k+\\&\frac{\partial}{\partial x_j}\left[\left(\mu+\sigma_k\mu_t\right)\frac{\partial k}{\partial x_j}\right]\end{aligned} \tag{3}$$

$$\begin{aligned}&\frac{\partial(\rho\omega)}{\partial t}+\frac{\partial\left(\rho u_j\omega\right)}{\partial x_j}=\frac{\gamma}{\nu_t}P-\beta\rho\omega^2+\\&\frac{\partial}{\partial x_j}\left[\left(\mu+\sigma_k\mu_t\right)\frac{\partial\omega}{\partial x_j}\right]+2\left(1-F_1\right)\frac{\rho\sigma_{\omega 2}}{\omega}\frac{\partial k}{\partial x_j}\frac{\partial\omega}{\partial x_j}\end{aligned} \tag{4}$$

Here, v_t is the turbulent viscosity due to eddy viscosity, represented as follows:

$$v_t=\frac{a_1 k}{\max(a_1\omega;\Omega F_2)} \tag{5}$$

In the above equations, $\sigma_k, \sigma_{\omega 2}, \beta, \beta^*, k, \gamma$ are constants, chosen differently for near-wall and far-from-wall flows.

This utilized the licensed commercial software ANSYS Fluent for simulation. The COUPLED algorithm was selected with a convergence criterion set at a residual tolerance of 10^{-6}, along with a second-order upwind scheme for both time and space. The numerical domain is defined with dimensions of $36.5D \times 22D \times 22D$ in the x, y, and z directions, as illustrated in Fig. 2. The domain length is carefully chosen to ensure accurate capture of the wake flow. The boundary conditions for subsonic and supersonic flows within the computational domain are summarized in Table 1.

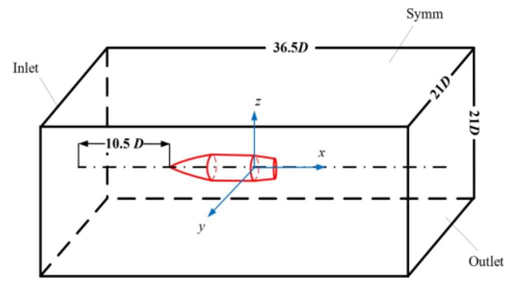

Fig. 2. Numerical domain

Table 1. Numerical conditions

Condition	Inlet	Outlet	Model
Subsonic	Velocity inlet	Pressure outlet	Wall
Supersonic	Pressure far field	Pressure outlet	Wall

2.3. Mesh Structure around the Model

In this study, a structured mesh is generated to ensure computational accuracy. A fine mesh with a growth ratio of 1.05 is applied near the model surface to capture boundary layer effects effectively. The first layer thickness away from the model is set at 0.2×10^{-7} m, ensuring accurate turbulence modeling. Fig. 3 illustrates an example of the mesh distribution around a boattail body with a boattail angle β of 7° and the length-to-diameter ratio of the boattail (L_D/D) of 1.0.

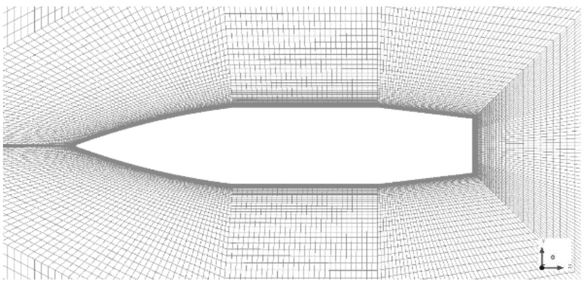

Fig. 3. Mesh around the model with β = 7° and L_D/D = 1.0

Fig. 4 presents the drag coefficient of the 7° boattail model with different mesh volumes. The Mach number in this case was 1.5. The difference in the results is not large with a maximum of 2% in comparison of the coarse mesh with the finest mesh. The drag coefficient decreases and reaches a constant value of 0.318 for mesh above 3.0 million cells. Consequently, the mesh cells of 3.6 million are selected for the all-numerical process for convergence of the results.

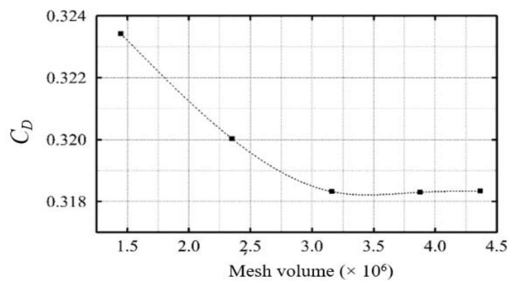

Fig. 4. Effect of cell number on the drag coefficient

Previously, the k-ω SST turbulence model shows an advantage model for simulation of the flow around the model with suitable numerical time. However, the results of this model are highly dependent on the two parameters of a_1 and β^* particularly for the surface flow. For that reason, in this current study, these two parameters are selected automatically using a UDF function. We tested two k-ω SST turbulence models by changing the bending functions. The results of the drag are presented in the next section.

2.4. Validation of the Numerical Method

Since the drag is the main important result of this study, the calculation of the drag is compared with experimental results for validation. Fig. 5 presents the results of the drag coefficient for the 7° boattail model. The relevant results of previous studies and calculations using Datcom software are also added. In our simulation, different methods for parameter adjustment are also presented. As can be seen, when the parameter is adjusted, numerical results show close to experimental data by Platou *et al*. [8]. Although the results at supersonic conditions are captured well, the Datcom software can not present good results for Mach number around 1.0. The numerical method, therefore, can be used to obtain the initial drag coefficient for the training.

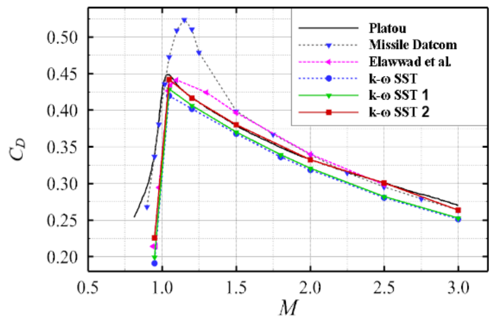

Fig. 5. Drag as a function of Mach number by different numerical method

3. Results and Discussions

3.1. Drag and Flow Behavior

Fig. 6 shows the results of the drag coefficient for different boattail angles and Mach numbers from subsonic to supersonic conditions. At subsonic conditions, the results are highly consistent for two Mach numbers of 0.1 and 0.7. It is understood that the flow behavior and wake structure change little for the flow at subsonic and therefore the trend of the drag is similar. At supersonic flow, the trend of the drag is highly modified. In detail, the drag decreases with increasing Mach number, and the boattail angle with minimum drag shifts to around 7-9°. These results are highly consistent with previous data by Cumming *et al*. [10] at supersonic flow and by Tran *et al*. [6] at subsonic conditions.

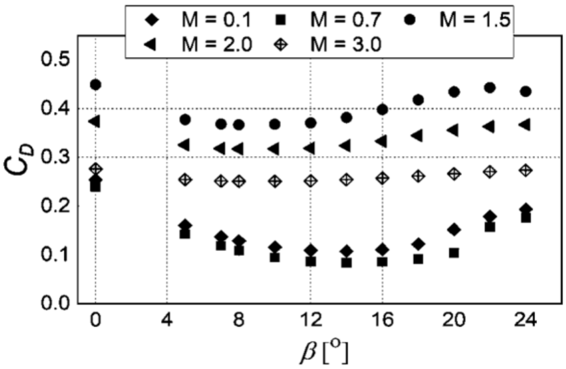

Fig. 6. Drag as a function of Mach number and boattail angles

Under transonic conditions, the trend of the drag for different boattail angles is similar at both Mach numbers of 0.95 and 1.05, except for the difference in the values (see Fig. 7). Here, the drag coefficient decreases and gets the minimum value at β of 8° and then it increases to a boattail angle of up to 20°. For the angles above 20°, a decrease in drag occurs again. The trend of the drag is connected to the position of the shock wave occurring on the rear region of the model. For more details, the surface flow will be analyzed in the next section. The results of the drag provide sufficient good data for the training process, which will be conducted.

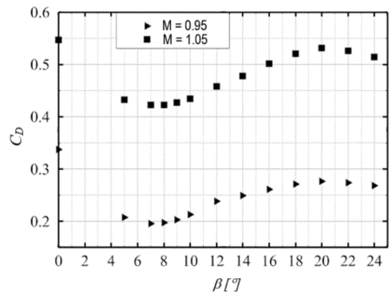

Fig. 7. Drag as a function of boattail angles at transonic conditions

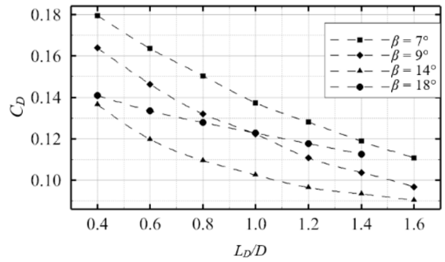

Fig. 8. Drag as function of boattail length (M = 0.1)

Fig. 8 illustrates the dependence of drag force on the boattail length at various boattail angles. At supersonic speeds, aerodynamic drag decreases significantly as the boattail length increases at small boattail angles β of 7° and 9°. When the boattail length is increased, the base area of the model reduces considerably, leading to a smaller wake and reduced base drag. However, at larger boattail angles ($\beta \geq 18°$), the drag changes very little with increasing boattail length. This could be due to flow separation occurring on the tail surface at larger boattail angles. At subsonic speeds, the results also show a similar trend with increasing boattail length. However, the influence of the boattail angle differs, corresponding to the change in flow conditions between supersonic and subsonic speeds. It is evident that despite changes in boattail length, the boattail angle with the lowest drag remains at 14° in the subsonic speed range. Therefore, the boattail length does not affect the value of the boattail angle with the lowest drag.

At subsonic speeds, a similar trend of decreasing drag with increasing boattail length is observed. At different boattail lengths, the boattail angle with the lowest drag is consistently 14° (Fig. 9). It can be seen that at the large boattail angle β of 18°, the drag changes very little. Additionally, at L_D/D of 0.4, the difference in drag between the two boattail angles β of 14° and 18° is not significant. However, the difference in drag between these two angles tends to increase as the boattail length increases. Similar to the supersonic case, at large boattail angles, flow separation occurs on the tail surface, generating high drag. The influence of boattail length on drag at large boattail angles is small.

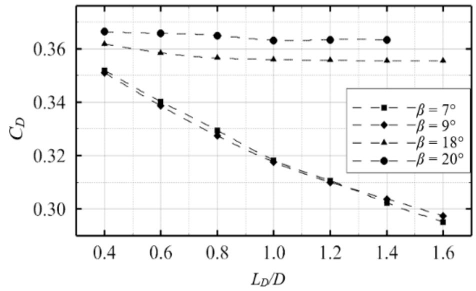

Fig. 9. Drag as function of boattail length at M = 2.0

The flow behavior around the boattail model is presented in Fig. 10 for different Mach number conditions for two typical boattail angles of 7° and 14°. It can be seen that the flow around the model changes largely with the boattail model and Mach conditions. A large difference occurs for the subsonic and supersonic conditions. In detail, the flow is highly curvature and smooth at subsonic conditions for both two configurations. This is due to the smooth change of the flow. An increase in the velocity occurs around the leading edge of the boattail, which is due to the change of the geometry there. However, at supersonic flow, the existence of the shock wave can be seen clearly for boattail angles and makes the flow highly modified. At a boattail angle of 7°, the shock wave is weak with two main shocks occurring at the leading edge and trailing edge of the boattail. However, it becomes remarkably strong at the angle of 14° and the shock wave occurs mainly at the leading edge of the model.

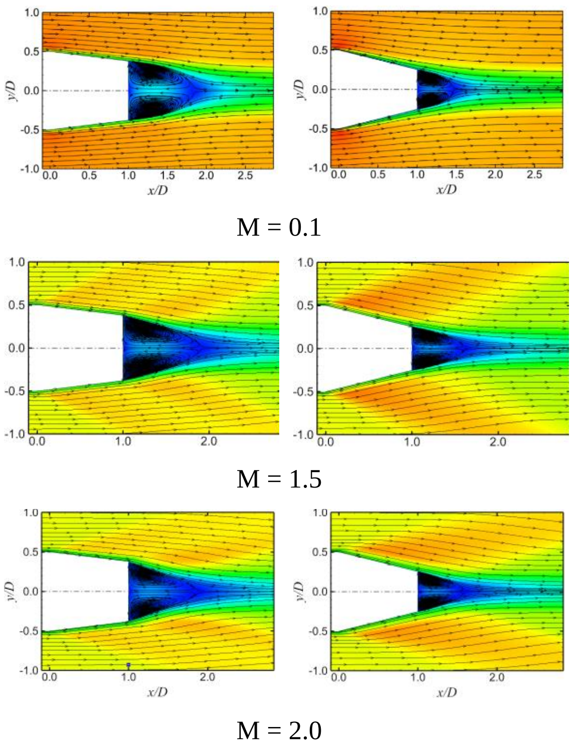

Fig. 10. Flow around the boattail model (left - β =7°, right - β =14°)

3.2. Selection of Neuron Networks and Evaluation of Uncertainty

To predict the drag coefficient of the model, a neural network is built. The neural network utilizes continuous transformations from input data passing through hidden layers via linear transformations, represented by the formula below:

$$z = w_1x_1 + w_2x_2 + w_3x_3 + ... + w_nx_n + b = \sum_{i=1}^{n} w_ix_i + b \quad (6)$$

Here, w_i represents the weights of the input variables, x_i denotes the input variables, n is the number of input variables, and b is the bias adjustment coefficient. The bias adjustment coefficient functions akin to additional neurons that are not directly connected to preceding layers. By utilizing bias adjustment coefficients, we can dynamically shift the activation function position at neurons to the right or left, enhancing the flexibility of the network's training process and potentially boosting its efficiency.

After traversing the hidden layer, the neural network proceeds to employ nonlinear transformations facilitated by activation functions. These functions play a pivotal role in both the training and operation of artificial neural networks, defining their nonlinear characteristics and learning capabilities. Various activation functions exist, with the following being commonly employed for predicting aerodynamic coefficients [11] as below:

Sigmoid Function (*Logsig*):

$$\sigma(z) = \frac{1}{1+e^{-z}} \quad (7)$$

Hyperbolic Tangent Sigmoid Function (*tanh*):

$$\sigma(z) = \frac{e^z - e^{-z}}{e^z + e^{-z}} \quad (8)$$

Loss Function optimization involves adjusting the parameters of the ANN to minimize its value. This optimization task is commonly accomplished using specialized algorithms. Various algorithms can be utilized for this purpose, including Levenberg-Marquardt (LM), Bayesian Regularization (BR), and Gradient Descent with Momentum (GD), among others. In this study, we opt for the LM algorithm, as previous research has demonstrated its efficacy in predicting aerodynamic coefficients [12, 13].

The network structure is shown in Fig. 12. In the study, a single-hidden-layer ANN is selected due to its simplicity while still ensuring the reliability of the obtained results, according to [14]. The input layer includes the length of the boattail, its angle, and the Mach number of the flow. This study used one hidden layer and the output is the drag coefficient. The number of neurons in the hidden layer can be modified. To evaluate the stability of the neuron number on the results, different tests were conducted. Here, the number of neurons is changed from 2 to 200.

In order to evaluate the uncertainty of the network, two parameters Mean Absolute Error (*MAE*) and Coefficient of Determination (*R*) are calculated by the following equations:

$$MAE = \frac{1}{n}\sum_{i=1}^{n}\left|y_i - y_{ANNi}\right| \tag{9}$$

$$R = 1 - \frac{\frac{1}{n}\sum_{i=1}^{n}(y_i - y_{ANNi})^2}{\frac{1}{n}\sum_{i=1}^{n}(y_i - \bar{y})^2} \tag{10}$$

The *MAE* close to zero shows good parameters of the network while the *R* close to one is better. The error shows the difference in mean value between the training and test data. As can be seen, when the number of parameters in the network increases, the error becomes smaller up to *n* equal to 40. With further increasing *n*, the error increases again. For that purpose, this study used 30 neurons for the network. Note that the error of the network in predicting the drag coefficient is less than 0.3%. Next, the effect of the training algorithm and activation function of the results are investigated. The results are shown in Tables 2, 3, and 4. From the results, the BR algorithm and ReLU activation function are selected.

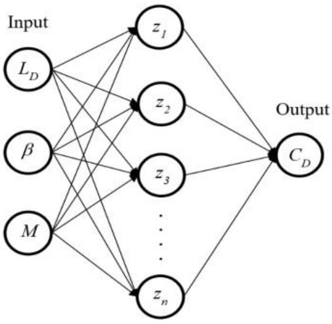

Fig. 12. Design of the neural network

Table 2. Effect of neuron number on the uncertainty

Test number	Neurons number	MAE	R	Error (%)
1	2	0.003	0.9832	8.86
2	5	0.004	0.9997	1.24
3	10	9.491×10^{-4}	1	0.42
4	15	7.926×10^{-4}	1	0.25
5	20	8.043×10^{-4}	1	0.25
6	25	7.419×10^{-4}	1	0.23
7	30	6.638×10^{-4}	1	0.19
10	35	7.124×10^{-4}	1	0.22

Table 3. Effect of training on the uncertainty

Training function	MAE	R	Error (%)
BR	6.638×10^{-4}	1	0.19
LM	0.023	0.9884	2.61
GD	0.161	0.8897	27.68

Table 4. Effect of activate function on the error of the network

Activate function	MAE	R	Error (%)
Sigmoid	6.6379×10^{-4}	1	0.19
Tanh	0.0011	1	0.24
ReLU	0.00191	0.9872	0.29

Fig. 13 presents several results from the training process, including the convergence and error history. It can be observed that overfitting does not occur, and the Mean Square Error (*MSE*) function exhibits good convergence. Additionally, the Coefficient of Determination (*R*) approaches a value of 1, indicating that the network's predictions account for a significant portion of the variability in the input and numerical output data.

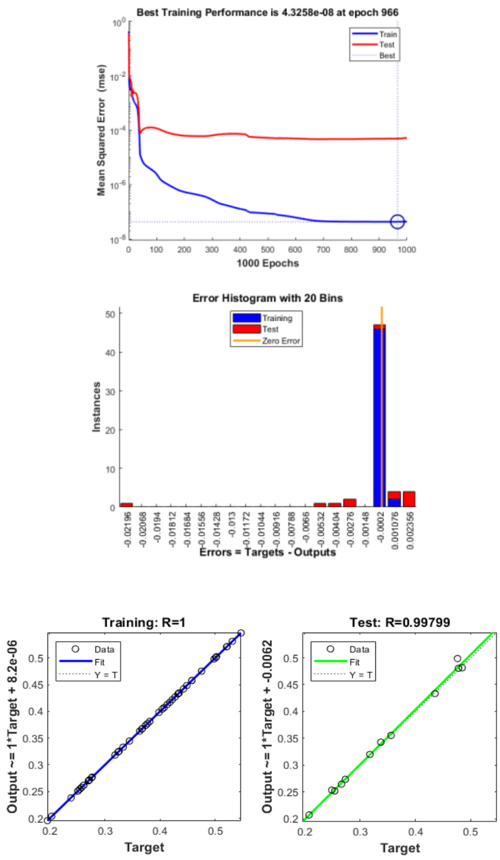

Fig. 13. ANN convergence and error history

Fig. 14 presents the results of the drag coefficient from ANN and Computational Fluid Dynamics (CFD) for different boattail angles at a Mach number of 2.0. A high consistency of the results is obtained for the two methods. The maximum difference of the results is less than 2%. When the parameters are carefully checked and selected, the ANN should be a good method for predicting the aerodynamic drag of the axisymmetric boattail model. Next, the network is extended for other cases of Mach number to find the boattail angles with minimum drag.

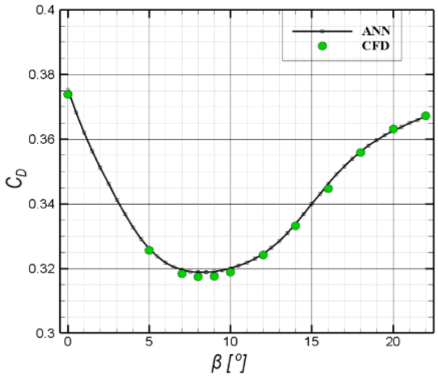

Fig. 14. Drag by CFD and ANN

3.3. Drag of the Model Using Neural Network

The predicting results of the drag for two different flow conditions are shown in Fig. 13. Here, the *x*-axis shows the boattail angle while the *y*-axis presents the length of the boattail. Clearly, the drag trend is similar for two Mach number conditions and the length of the boattail has a large effect on the drag behavior.

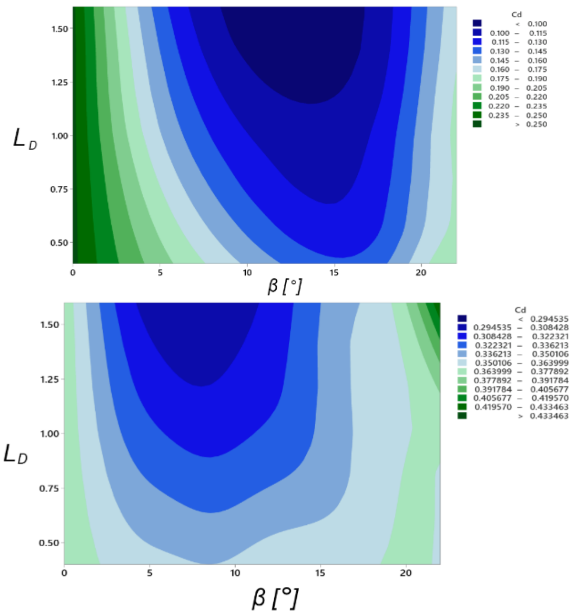

Fig. 15. Results of the drag by ANN (upper: subsonic flow, lower: supersonic flow)

The results also indicate that the angle with minimum drag is around 12-16° at subsonic conditions and shifts to 6-8° at supersonic flow. In comparison to the supersonic flow, the drag at subsonic conditions changes much larger. Consequently, using boattail is sufficiently effective in subsonic flow in comparison to the case of supersonic conditions. This interesting result was not presented in previous investigations. In the next study, a convolutional neural network is developed for predicting the flow fields and pressure distribution around the model.

4. Conclusions

This study focuses on the drag of the axisymmetric boattail model by neural network. To obtain the data for the training process, CFD was developed. In detail, the RANS with the modified *k-ω* turbulent model was applied for the simulation to obtain initial data for the training process. The results revealed that the numerical data is highly consistent with experimental results. The main conclusion of this study is as below.

At subsonic flow, the angle with minimum drag is around 14° but it dramatically shifts to 7-9° at supersonic conditions. The minimum drag is less sensitive to the boattail angle, while the drag reduces as the boattail length increases.

The maximum error of the neural network in predicting aerodynamic drag is less than 2%. Consequently, it can be used in further study to predict the aerodynamic drag of the model.

The existence of minimum drag at supersonic flow is due to the generation of shock waves around the boattail, which has a large effect on the pressure and drag trend.

This study provides a good reference for further design of axisymmetric flying objects and proposes a good control method for drag reduction.

Acknowledgments

This research is funded by Vietnam National Foundation for Science and Technology Development (NAFOSTED) under grant number 107.03-2021.52.

References

[1] T. H. Tran, T. Ambo, T. Lee, L. Chen, T. Nonomura, and K. Asai, Effect of boattail angles on the flow pattern on an axisymmetric afterbody surface at low speed, Experimental Thermal Fluid Science, vol. 99, pp. 324-335, Dec. 2018. https://doi.org/10.1016/j.expthermflusci.2018.07.034

[2] The Hung Tran, Takumi Ambo, Taekjin Lee, Yuta Ozawa, Lin Chen, Taku Nonomura & Keisuke Asai, Effect of Reynolds number on flow behavior and pressure drag of axisymmetric conical boattails at low speeds, Experiments in Fluids, vol. 60, pp. 1-19, Feb. 2019. https://doi.org/10.1007/s00348-019-2680-y

[3] W. A. Mair, Reduction of base drag by boat-tailed afterbodies in low speed flow, Aeronautical Quarterly, vol. 20, iss. 4, pp. 307-320, Jun. 2016. https://doi.org/10.1017/S0001925900005126

[4] P. R. Viswanath, Flow management techniques for base and afterbody drag reduction, Progress in Aerospace Sciences, vol. 32, iss. 2-3, pp. 79-129, 1996. https://doi.org/10.1016/0376-0421(95)00003-8

[5] A. Mariotti, G. Buresti, G. Gaggini, and M. V. Salvetti, Separation control and drag reduction for boat-tailed axisymmetric bodies through contoured transverse grooves, Journal of Fluid Mechanics, vol. 832, pp. 514-549, Oct. 2017. https://doi.org/10.1017/jfm.2017.676

[6] T. H. Tran, H. Q. Dinh, H. Q. Chu, V. Q. Duong, C. Pham, and V. M. Do, Effect of boattail angle on near-wake flow and drag of axisymmetric models: a numerical approach, Journal of Mechanical Science and Technology, vol. 35, pp. 563-573, Jan. 2021. https://doi.org/10.1007/s12206-021-0115-1

[7] R. Thirumalainambi and J. Bardina, Training data requirement for a neural network to predict aerodynamic coefficients, Independent Component Analyses, Wavelets, and Neural Networks, vol. 5102, pp. 92-103, Apr. 2003. https://doi.org/10.1117/12.486343

[8] A. S. Platou, Improved projectile boattail, J. Spacecraft Rockets, vol. 12, no. 12, pp. 727-732, Dec. 1975. https://doi.org/10.2514/3.57040

[9] F. R. Menter, Two-equation eddy-viscosity turbulence models for engineering applications, AIAA Journal, vol. 32, no. 8, pp. 1598-1605, Aug. 1994. https://doi.org/10.2514/3.12149

[10] R. M. Cummings, H. T. Yang, and Y. H. Oh, Supersonic, turbulent flow computation and drag optimization for axisymmetric afterbodies, Computers and Fluids, vol. 24, iss. 4, pp. 487-507, 1995. https://doi.org/10.1016/0045-7930(94)00040-6

[11] J. Feng and S. Lu, Performance analysis of various activation functions in artificial neural networks, in Journal of Physics: Conference Series, vol. 1237, iss. 2, pp. 22030, 2019. https://doi.org/10.1088/1742-6596/1237/2/022030

[12] D. F. Kurtulus, Ability to forecast unsteady aerodynamic forces of flapping airfoils by artificial neural network, Neural Computing Applications, vol. 18, pp. 359-368, Apr. 2008. https://doi.org/10.1007/s00521-008-0186-2

[13] T. Rajkumar, C. Aragon, J. Bardina, and R. Britten, Prediction of aerodynamic coefficients for wind tunnel data using a genetic algorithm optimised neural network, WIT Transaction on Information and Communication Technology, vol. 28, 2002.

[14] M. Carpente, R. Hartfield, J. Burkhalter, A comprehensive approach to cataloging missile aerodynamic performance using surrogate modeling techniques and statistical learning, in 29th AIAA Applied Aerodynamics Conference, Honolulu, HI, USA, Jun. 27-30, 2011, pp. 3029. https://doi.org/10.2514/6.2011-3029